ISSN 1063-7834, Physics of the Solid State, 2022. © Pleiades Publishing, Ltd., 2022.
Russian Text © The Author(s), 2021, published in Fundamental'nye Problemy Sovremennogo Materialovedeniya, 2021, Vol. 18, No. 2, pp. 154–164.

Study of the Structure and Properties of a High-Entropy AlCoCrFeNi Alloy after Electron-Beam Processing

Yu. F. Ivanov[a], V. E. Gromov[b], S. V. Konovalov[b], Yu. A. Shliarova[b, *], K. A. Osintsev[c], and I. A. Panchenko[b]

[a] *Institute of High Current Electronics, Siberian Branch, Russian Academy of Sciences, Tomsk, 634055 Russia*
[b] *Siberian State Industrial University, Novokuznetsk, 654007 Russia*
[c] *Samara National Research University, Samara, 443086, Russia*
**e-mail: rubannikova96@mail.ru*

Received March 5, 2021; revised June 29, 2021; accepted June 29, 2021

Abstract—Using wire-arc additive manufacturing (WAAM), we produced samples of Al–Co–Cr–Fe–Ni high-entropy alloy (HEA) with a grain size of 4–15 μm. Inclusions of the second phase were found along the boundaries and in the volume of the grains. The near-boundary volumes of the alloy (volumes located along grain boundaries) are enriched in chromium and iron atoms, the volume of grains is enriched in nickel and aluminum atoms, and cobalt is quasi-uniformly distributed in the alloy. The inclusions of an elongated shape are enriched in chromium, iron, and oxygen atoms and may be carbides. Microhardness, modulus of elasticity, and tribological properties of the alloy are determined and the stretch curves are analyzed. Irradiation of the HEA with a pulsed electron beam is accompanied by the release of grain boundaries from precipitates of the second phase, which indicates the homogenization of the material. High-speed crystallization of the molten surface layer of HEA samples is accompanied by the formation of a columnar structure with a submicrometer-nanocrystalline structure. The electron-beam processing decreases the microhardness of the surface layer of the alloy with a thickness of up to 90 μm, which may be due to the relaxation of internal stress fields formed in the initial material during its manufacture. Irradiation of a high-entropy alloy with an intense pulsed electron beam improves the strength and plasticity of the material, increasing the compressive strength by 1.1–1.6 times.

Keywords: wire-arc additive manufacturing, AlCoCrFeNi high-entropy alloy, properties, structure, electron-beam processing

DOI: 10.1134/S1063783422080042

INTRODUCTION

At the beginning of the 2000s, the creation and comprehensive study of new so-called high-entropy polymetallic alloys, including 5–6 or more basic elements, were reported [1–8].

The idea behind high-entropy alloys (HEAs) is that the atoms of all elements are considered to be atoms of the solute, cause deformation of the crystal structure, and improve the thermodynamic stability of properties associated with differences in the atomic radii of the components. This results in a high system entropy to further produce material with unique properties that are impossible with conventional microalloying methods.

The original results obtained in the field of HEA until 2015 are reviewed [9–13], where the thermodynamics of HEA is described, the results of modeling their structure are considered, and new variants of methods for obtaining multicomponent alloys are discussed.

Almost all types of such alloys are being developed (structural, cryo-resistant, heat-resistant, corrosion-resistant, with special magnetic and electrical properties), as well as compounds (carbides, nitrides, oxides, borides, silicides). In most cases, one can obtain a single-phase high-entropy material or a multi-phase material consisting of a multicomponent matrix and inclusions, which result in dispersion strengthening [14, 15].

However, further studies demonstrated that high-entropy alloys could have a more complex structure, consisting of a simple solid solution and a combination of intermetallic [16], amorphous [17], and nanocrystalline [18] phases.

Modern technologies for the production of high-entropy alloys can be conventionally divided into solid-state [19] and liquid processing methods [20], technologies for the deposition of thin films and coatings [21, 22], and additive production [23, 24].

The HEA properties can be improved by treating the surface with focused energy flows. Electron-beam processing is one of the most promising and highly efficient methods for the surface hardening of products [25, 26]. Electron-beam processing ensures ultrahigh heating rates (up to 10^6 K/s) of the surface layer to the specified temperatures and cooling of the surface layer due to heat removal to the main volume of the material at rates of 10^4–10^9 K/s, resulting in the formation of nonequilibrium submicrometer and nanocrystalline structural-phase states.

The goal of this work is to study the structural-phase state and properties of a high-entropy AlCoCrFeNi alloy subjected to electron-beam processing.

EXPERIMENTAL

To obtain a high-entropy alloy, we used the technology of wire-arc additive manufacturing (WAAM) [27]. Samples of high-entropy alloys were fabricated by layer-by-layer deposition on a steel substrate using wire-arc additive manufacturing under argon (99.99%). The starting material was a three-core cable made of aluminum wire (Al 99.95%, diameter 0.5 mm), chromium–nickel wire (Cr 20%, Ni 80%, diameter 0.4 mm), and nickel–cobalt wire (Co 17%, Fe 54%, Ni 29%, diameter 0.4 mm). The layers were deposited under the following conditions: cable feed speed 8 m/min, voltage 17 V, burner speed 0.3 m/min, and substrate temperature 523 K. The sample was made in the form of a parallelepiped 60 × 140 × 20 mm in size and consisted of 20 weld layers in height and 4 layers in width.

The elemental and phase composition of the alloy and the state of the defect substructure were studied by scanning electron microscopy (LEO EVO 50 microscope (Carl Zeiss) with an INCA-energy energy-dispersive analyzer and a TESCAN VEGA microscope with an INCAx-act energy-dispersive analyzer) and transmission electron diffraction microscopy (JEM 2100 instrument (JEOL)). The phase composition and state of the crystal lattice of the main phases of the HEA samples were studied by X-ray phase and X-ray diffraction analysis (X-ray XRD 6000 diffractometer (Shimadzu) and DRON-7); the recording was carried out in copper filtered Cu$K_{\alpha 1}$ radiation. The phase composition was analyzed using the PDF 4+ databases and the PowderCell 2.4 full-profile analysis program.

The mechanical properties of the HEA were characterized by the value of microhardness determined using an HV-1000 microhardness tester and nanohardness (NanoScan-4D nanotester). The measurements were carried out both along the deposited layers and in a perpendicular cross section to determine the degree of mechanical homogeneity of the material.

Tribological properties (wear resistance and friction coefficient) were determined on flat samples using a Pin-on-Disc and Oscillating TRIBOtester tribometer (TRIBOtechnic, France) with the following parameters: Al_2O_3 ceramic ball 6 mm in diameter, sample rotation speed 25 mm/s, the path traveled by the counterbody 100 m, indenter load 5 N, wear track radius 2 mm, room temperature, normal humidity. The wear of the material was determined from the results of the profilometry of the track formed during the tests.

The electron beam processing was carried out with the following parameters: accelerated electron energy $U = 18$ keV, electron beam energy density $E_s = 10$, 15, 20, 25, and 30 J/cm^2, electron beam pulse duration $t = 200$ μs, number of pulses $N = 3$. Irradiation was carried out in vacuum at a residual gas pressure (argon) in the installation chamber of $p = 0.02$ Pa.

RESULTS AND DISCUSSION

Images of the microstructure of the HEA sample made it possible to determine that the deposited layers have a dendritic structure. The grain sizes of the alloy vary from 4 to 15 μm. Inclusions of the second phase were found along the boundaries and in the volume of the grains.

Using the mapping methods, we found that the near-boundary volumes of the alloy (volumes located along grain boundaries) are enriched in chromium and iron atoms, the volume of grains is enriched in nickel and aluminum atoms, and cobalt is quasi-uniformly distributed in the alloy.

Energy dispersive X-ray spectroscopy of the cross section of the samples, performed every 5 mm, suggested that these elements are distributed uniformly throughout the entire volume of the material in the following composition: Al 35.67 ± 1.34 at %, Ni 33.79 ± 0.46 at %, Fe 17.28 ± 1.83 at %, Cr 8.28 ± 0.15 at %, Co 4.99 ± 0.09 at %. However, an increase in the iron concentration by 10% relative to its concentration in the bulk of the material was revealed at the boundary with the substrate. This may be because, in the process of wire-arc additive manufacturing, the deposited metal and the substrate material are mixed. No increase in the iron concentration was detected at a distance of 5 mm from the conditional boundary with the substrate, and the size of the deposited layer reaches 3 mm; therefore, we concluded that the substrate affects the chemical composition of only the first layer. The thermogravimetric analysis determined the melting point of the resulting HEA at 1495.18°C.

To reveal patterns of structure formation, we prepared samples from three regions located at different distances from the substrate: 15, 35, and 55 mm. These samples were studied by X-ray diffraction analysis. Comparison of the obtained X-ray patterns did not reveal a shift in the diffraction peaks, nor a change in

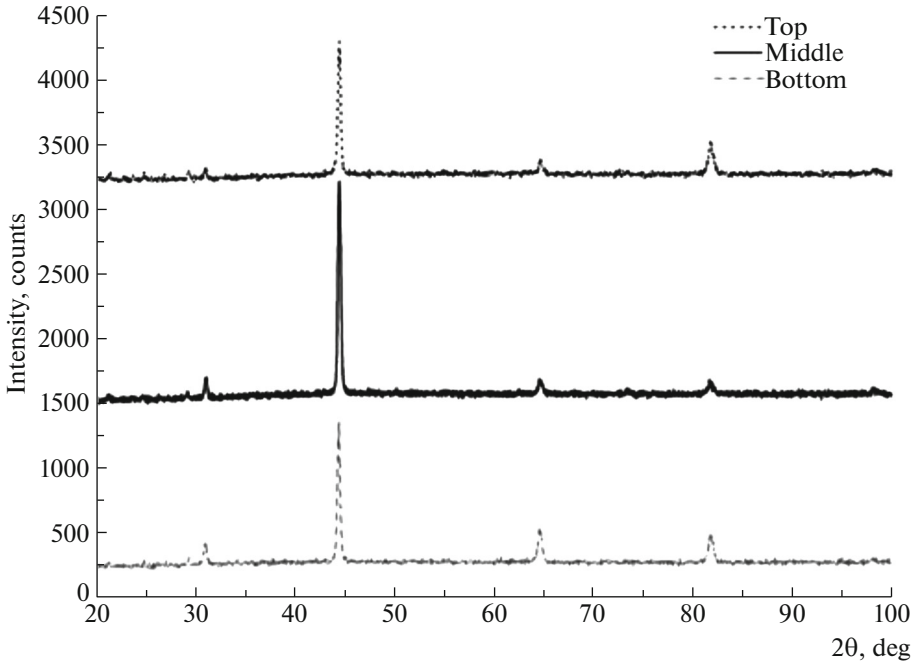

Fig. 1. X-ray diffraction patterns obtained in different regions (top, middle, and bottom) of the HEA sample.

the ratio of the intensity of the diffraction peaks to the intensity of the maximum peak was detected (Fig. 1). The results indicate the homogeneity of the phase composition of the produced high-entropy alloy.

By indexing the diffraction patterns, it was found that the crystal lattice of the sample has a cubic system. The detected diffraction maxima are described within the framework of one crystal lattice, namely, $Fe_{0.258}Ni_{1.164}Al_{0.578}$; chemical formula $Fe_{0.54}Ni_{0.836}Al_{0.624}$; empirical formula $Al_{0.624}Fe_{0.54}Ni_{0.836}$; wt % formula $Al_{17.53}Fe_{31.39}Ni_{51.08}$; at % formula $Al_{31.20}Fe_{27.00}Ni_{41.80}$; compound name aluminum–iron–nickel crystal (symmetry allowed): centrosymmetric; AC space group Pm-3m (221); Pearson symbol cP2.00; LPF prototype structure [formula order] CsCl, cP2,221. The crystal lattice parameter of this phase is 0.28914 nm.

However, one should also take into account the results obtained by scanning electron microscopy, prooving the multiphase nature of the alloy. The results of a qualitative analysis of the diffraction pattern, taking into account these facts, suggest the following phase composition of the alloy. Quantitative phase analysis showed the following phase ratio: AlNi 36.56%, CrFe 27.02%, Al_2FeCo 36.42%.

Transmission electron microscopy analysis of the alloy structure made it possible to study the distribution of the elemental composition, the state of the defective substructure, and the morphology of the phases of the material at the submicrometer- and nanoscale levels. We found that the alloy contains inclusions of two size classes: submicrometer inclusions (Figs. 2a–2c) and nano-sized inclusions (Fig. 2d, particles are indicated by arrows).

The Vickers method determined the value of microhardness at 474 ± 8 HV. The Rockwell hardness measured in three regions located at distances of 50, 30, and 10 mm from the substrate was 47 ± 5 HRC on average. The resulting hardness is comparable to that of steel 45 (45 HRC).

The nanohardness of the test sample is on average 10.4 ± 0.8 GPa, regardless of the distance from the surface. The elastic modulus measured by nanoindentation is 304 ± 15 GPa. The test performed made it possible to find the HEA wear coefficient is 1.4×10^{-4} mm^3/N m; the friction coefficient is 0.65.

To implement tests by uniaxial compression, cylindrical samples 10 mm in height and 5 mm in diameter were cut from a bulk HEA billet by the electroerosive method. For uniaxial tensile tests, specimens were made with a thickness of 2.3 mm, a width of 9.1 mm, and a length of the working part of 16.0 mm. The results of compressive testing of HEA samples showed that the ultimate strength of the material is in the range of 1400–1900 GPa. Young's modulus has a value of 273–372 GPa (Fig. 3).

When analyzing the images of the HEA surface structure formed upon irradiation with a pulsed electron beam of different energy densities, the following features of structure formation were noted.

First, we should note that, regardless of the energy density of the electron beam, the irradiation of HEA is accompanied by fragmentation of the sample surface

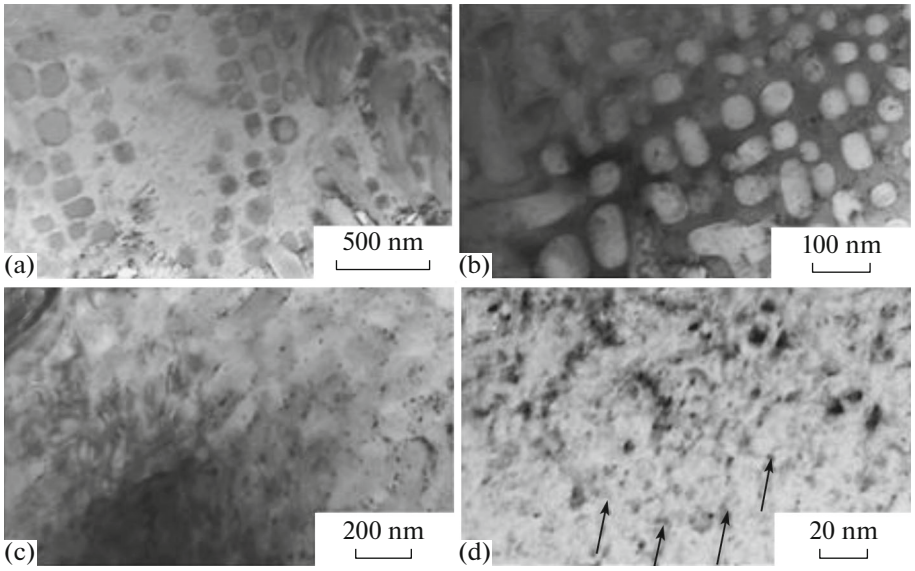

Fig. 2. Electron microscopic images of the HEA structure obtained in the study of thin foils.

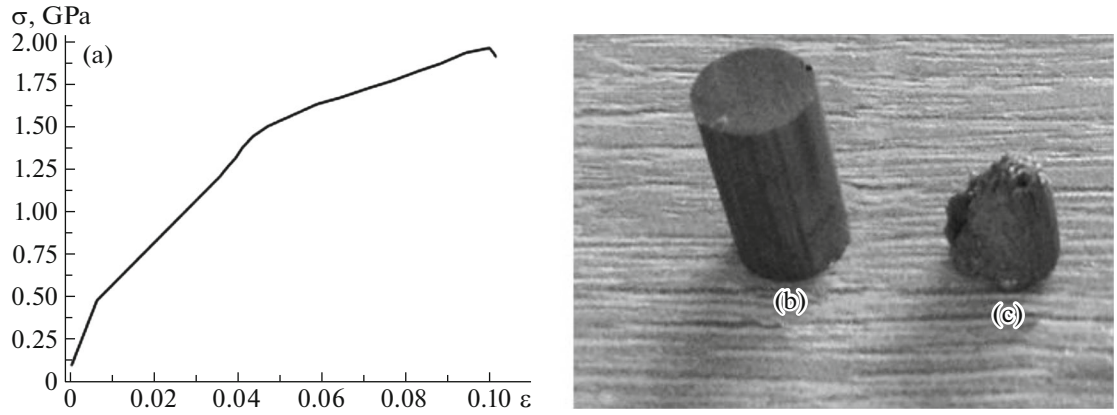

Fig. 3. (a) Curve of strain hardening of the specimen tested under uniaxial compression. Typical view of the samples (b) before and (c) after testing.

by a network of microcracks. The fragment sizes reach several hundred micrometers, significantly exceeding the grain sizes of the initial alloy. Microcracks are formed by the relaxation of elastic stress arising in the surface layer of the material during high-speed cooling, which takes place under conditions of irradiation with a pulsed electron beam of submillisecond duration. The relaxation of elastic stress through the formation of microcracks is characteristic of ceramic materials and indicates an increased fragility of the HEA under study.

Irradiation of HEA with a pulsed electron beam in the mode of melting of the surface layer is accompanied by homogenization of the material. This is evidenced by the release of the grain boundaries from the precipitates of the second phase. An increase in the energy density of the electron beam intensifies the process of formation of an alloy homogeneous in elemental composition.

High-speed crystallization of the molten surface layer of HEA samples is accompanied by the formation of a submicrometer-nanocrystalline structure. The sizes of crystallites increase with an increase in the energy density of the electron beam, and, at E_s = 30 J/cm^2, they vary from 100 to 200 nm (Fig. 4).

The irradiation of the alloy with a pulsed electron beam in the mode of melting of the surface layer can cause an uncontrolled change in the elemental composition of the material. The X-ray electron-probe microanalysis of the elemental composition of the HEA surface layer irradiated by a pulsed electron beam did not confirm this suggestion.

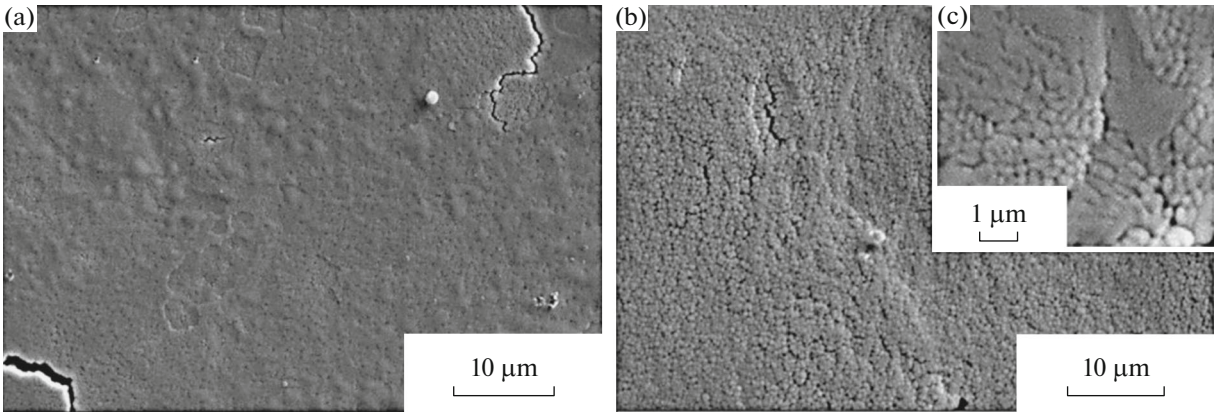

Fig. 4. Electron microscopic image of the structure of the HEA surface irradiated with a pulsed electron beam (200 μs, 3 pulses) at an electron beam energy density of 30 J/cm^2.

Scanning electron microscopy was used to study the structure of the brittle fracture surface of HEA samples modified by a pulsed electron beam. High-speed crystallization of the surface layer of the alloy leads to the formation of a columnar structure, a typical image of which is shown in Fig. 5.

The thickness of the modified layer (H) naturally increases from 0.8 to 20 μm with an increase in the energy density of the electron beam from 10 to 30 J/cm^2. The columnar structure is formed by crystallites, the sizes (h) of which increase regularly with an increase in the energy density of the electron beam. Thus, the energy density of the electron beam affects both the thickness of the modified layer and the size of crystallites formed as a result of processing.

The elemental composition of the samples irradiated with a pulsed electron beam was studied by the methods of X-ray electron-probe microanalysis of cross-sections. We found that the electron-beam processing yields a more uniform distribution of elements in the processed layer. For example, the enrichment of the volume of grains with aluminum and nickel, as well as the enrichment of grain boundaries with iron and chromium, observed in the untreated alloy, is not observed in the modified layer. Mapping of the cross section of the sample depending on the distance from the surface showed that the thickness of the homogenized layer reaches 4 μm. With increasing distance from the irradiation surface, the distribution of elements characteristic of the untreated sample is observed.

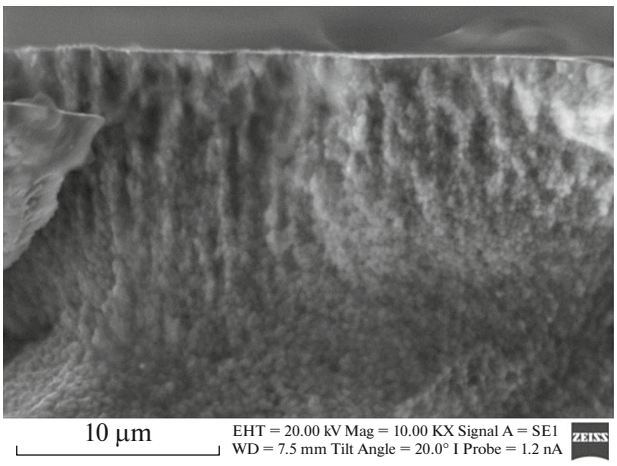

Fig. 5. SEM image of the structure of the HEA cleavage processed by a pulsed electron beam with an energy density of 30 J/cm^2.

The electron-beam treatment of the surface of the alloy samples at different energy densities of the electron beam led to a decrease in the microhardness of the surface layer, regardless of the treatment parameters. The values decreased by an average of 100 HV in the treated layer relative to the material bulk regions. The lowest value of microhardness was observed in the treatment mode with an electron beam energy density of 10 J/cm^2; it amounted to 368 ± 1 HV on the surface. The highest microhardness value of the treated surface, 403 ± 6 HV, was found in the material treated with an electron beam energy density of 25 J/cm^2. The electron-beam treatment changes the microhardness of the surface layer to a depth of up to 90 μm.

The results of the study of nanohardness and elastic modulus of the treated samples revealed a correlation with the data on changes in microhardness; namely, the nanohardness and Young's modulus of the surface layer decreased by an average of 28–30%. This fact indicates that electron-beam processing leads to the relaxation of internal stress fields formed in the initial material during its manufacture.

The performed tribological tests of samples in the initial state and after electron-beam treatment in various modes showed that electron-beam treatment has little effect on the friction coefficient and wear rate.

The value of the sample wear rate without treatment is 1.4×10^{-4} mm^3/N m, and in those treated with an electron beam, the values vary from 1.4×10^{-4} to 2.5×10^{-4} mm^3/N m.

CONCLUSIONS

In the last two decades, the attention of scientists involved in solid-state physics has been drawn to the study of high-entropy alloys. Using the technology of wire-arc additive manufacturing, samples of a high-entropy alloy (HEA) were made. A multicomponent wire consisting of three strands of different elemental compositions was used as the starting material. The resulting alloy has the following elemental composition (wt %): 15.64 Al, 7.78 Co, 8.87 Cr, 22.31 Fe, and 44.57 Ni and corresponds to a nonequimolar high-entropy alloy of the Al–Co–Cr–Fe–Ni system. The optical microscopy and scanning electron microscopy of a transverse etched section demonstrated that the deposited layers have a dendritic structure. The grain sizes of the alloy vary from 4 to 15 μm. Inclusions of the second phase were found along the boundaries and in the volume of the grains. Using the mapping methods, we found that the near-boundary volumes of the alloy (volumes located along grain boundaries) are enriched in chromium and iron atoms, the volume of grains is enriched in nickel and aluminum atoms, and cobalt is quasi-uniformly distributed in the alloy. The melting temperature of the resulting high-entropy alloy, determined by thermogravimetry, is 1495.18°C. X-ray diffraction analysis revealed the homogeneity of the phase composition of the manufactured high-entropy alloy. The crystal lattice parameter of this phase is 0.28914 nm.

The elastic modulus measured by nanoindentation is 304 ± 15 GPa. The tribological tests yielded the HEA wear coefficient of 1.4×10^{-4} mm^3/N m; the friction coefficient is 0.65. The average microhardness values are 474 ± 8 HV. The tensile strength of the material is in the range of 1400–1900 MPa.

Irradiation of the HEA with a pulsed electron beam is accompanied by the release of grain boundaries from precipitates of the second phase, which indicates the homogenization of the material. The phase composition of the alloy does not change in this case. High-speed crystallization of the molten surface layer of HEA samples is accompanied by the formation of a columnar structure with a submicrometer-nanocrystalline structure. Using X-ray electron-probe microanalysis, we proved that the elemental composition of the surface layer of the alloy is practically independent of the energy density of the electron beam and, within the measurement error, corresponds to the elemental composition of the initial material.

Irradiation of a high-entropy alloy with an intense pulsed electron beam improves the strength and plasticity of the material, increasing the compressive strength by 1.1–1.6 times. The highest compressive strength of 2179 MPa was obtained in the alloy treated with an electron beam with an energy density of 30 J/cm^2. The conditional compressive yield strength, in this case, was 522 MPa, and Young's modulus was 257 GPa.

FUNDING

This work was supported by the Russian Science Foundation, project no. 20-19-00452.

CONFLICT OF INTEREST

The authors declare that they have no conflicts of interest.

REFERENCES

1. E. P. George, W. A. Curtin, and C. C. Tasan, Acta Mater. **188**, 435 (2020).
2. V. Shivam, J. Basu, V. K. Pandey, Y. Shadangi, and N. K. Mukhopadhyay, Adv. Powder Technol. **29**, 2221 (2018).
3. U. L. Ganesh and H. Raghavendra, J. Therm. Anal. Calorim. **139**, 207 (2020).
4. Y. A. Alshataif, S. Sivasankaran, F. A. Al-Mufadi, A. S. Alaboodi, and H. R. Ammar, Met. Mater. Int. **26**, 1099 (2019).
5. K. C. Cheng, J. H. Chen, S. Stadler, and S. H. Chen, Appl. Surf. Sci. **478**, 478 (2019).
6. J. Joseph, P. Hodgson, T. Jarvis, X. Wu, N. Stanford, and D. M. Fabijanic, Mater. Sci. Eng. A **733**, 59 (2018).
7. R. Jian, L. Wang, S. Zhou, Y. Zhu, Y. J. Liang, B. Wang, and Y. Xue, Mater. Lett. **278**, 128405 (2020).
8. L. Hou, J. Hui, Y. Yao, J. Chen, and J. Liu, Vacuum **164**, 212 (2019).
9. Y. Zhang, T. T. Zuo, Z. Tang, M. C. Gao, K. A. Dahmen, P. K. Liaw, and Z. Lu, Prog. Mater. Sci. **61**, 1 (2014).
10. B. Cantor, Entropy **16**, 4749 (2014).
11. D. B. Miracle and O. N. Senkov, Acta Mater. **122**, 448 (2017).
12. W. Zhang, P. K. Liaw, and Y. Zhang, Sci. China Earth Sci. **61**, 2 (2018).
13. K. A. Osintsev, V. E. Gromov, S. V. Konovalov, Yu. F. Ivanov, and I. A. Panchenko, Izv. Ferr. Metall., No. 4, 1 (2021).
14. A. D. Pogrebnyak, A. A. Bagdasapuan, I. V. Yakushchenko, and V. M. Beresnev, Russ. Chem. Rev. **83**, 1027 (2014).
15. A. S. Rogachev, Phys. Met. Mater. Sci. **121**, 807 (2020).
16. M. H. Tsai, R. C. Tsai, T. Chang, and W. F. Huang, Metals (Basel) **9**, 1 (2019).
17. Y. Y. Zhao, Y. X. Ye, C. Z. Liu, R. Feng, K. F. Yao, and T. G. Nieh, Intermetallics **113**, 106561 (2019).
18. D. Oleszak, A. Antolak-Dudka, and T. Kulik, Mater. Lett. **232**, 160 (2018).

19. J. Wang, Y. Liu, B. Liu, Y. Wang, Y. Cao, T. Li, and R. Zhou, Mater. Sci. Eng. A **689**, 233 (2017).

20. N. Yurchenko, E. Panina, M. Tikhonovsky, G. Salishchev, S. Zherebtsov, and N. Stepanov, Int. J. Refract. Met. Hard Mater., 105322 (2020).

21. T. W. Lu, C. S. Feng, Z. Wang, K. W. Liao, Z. Y. Liu, Y. Z. Xie, J. G. Hu, and W. B. Liao, Appl. Surf. Sci. **494**, 72 (2019).

22. Y. Geng, S. V. Konovalov, and X. Chen, Prog. Phys. Met. **21**, 26 (2020).

23. Y. H. Zhou, Z. H. Zhang, Y. P. Wang, G. Liu, S. Y. Zhou, Y. L. Li, J. Shen, and M. Yan, Addit. Manuf. **25**, 204 (2019).

24. Y. A. Alshataif, S. Sivasankaran, F. A. Al-Mufadi, A. S. Alaboodi, and H. R. Ammar, Met. Mater. Int. **26**, 1099 (2019).

25. Yu. F. Ivanov, V. E. Gromov, D. V. Zagulyaev, S. V. Konovalov, Yu. A. Rubannikova, and A. P. Semin, Prog. Phys. Met. **21**, 345 (2020).

26. V. E. Gromov, Yu. F. Ivanov, S. E. Vorobiev, and S. V. Konovalov, *Fatigue of Steels Modified by High Intensity Electron Beams* (Cambridge Univ. Press, Cambridge, 2015).

27. Q. Shen, X. Kong, and X. Chen, J. Mater. Sci. Technol. **74**, 136 (2021).

Translated by O. Zhukova